Numerical Model of Electromagnetic Stirring for Continuous Casting Billets

Leonardo B. Trindade, Antônio C. F. Vilela, Ály F. F. Filho, Marco T. M. B. Vilhena, and Rodrigo B. Soares

Abstract—This paper introduces a numerical model of an electromagnetic rotary stirrer based on the finite-element model. Such stirrers are used to improve the quality of continuously cast steel, particularly billets and blooms. The method determines the magnetic flux density profile and compares it to experimental measurements. In addition, it calculates the Lorentz force field as a function of the stirrer position, the current applied, and the frequency. The stirrer position at the end of the mold affects the profile symmetry of the force, creating a z component of the force. With this model, it will be possible to simulate the fluid dynamics effects in the molten steel.

Index Terms—Continuous casting, electromagnetic stirring, finite-element model.

I. INTRODUCTION

ELECTROMAGNETIC stirring has been used in continuous casting plants for a long time. It has been applied both to slabs and billets but with different stirring principles. A good review can be found in the work of Tzavaras and Brody [1] and Birat and Choné [2].

There are few papers about numerical models of stirrers for billets [3]–[8], and most of them do not show the details of the device. Very little is known about the magnetic flux density distribution and the Lorentz force distribution in the billet cast.

The aim of this work is to build a model using the commercial package OPERA-3d/ELEKTRA that is based on the finite-element method. Experimental measurements of the magnetic flux density were carried out to validate the model. The Lorentz force vector distribution was obtained in the strand cast. These parameters were obtained for different values of current, frequency, and the stirrer position in the mold. The effect of the mold temperature on the electric conductivity is also analyzed.

II. ELECTROMAGNETIC STIRRING

Electromagnetic stirring is based on the induction motor principle where the steel is put in the place of the rotor. In general, the motion induced in the billets is rotary. The system is fed by a three-phase power source to produce a rotating magnetic field. This rotating magnetic field induces currents in the steel due to the conductive property of the metal. The product between
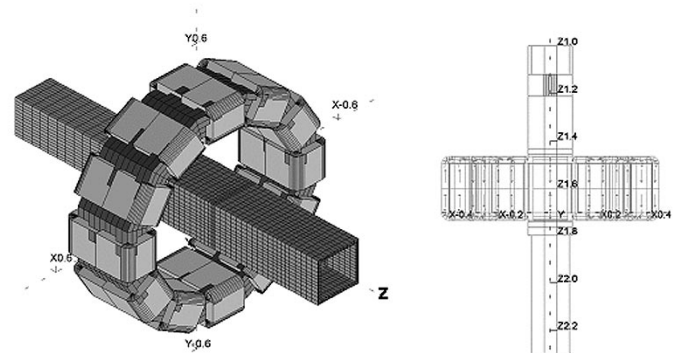
Fig. 1. Model geometry and the finite-element mesh.

this field and the currents gives the Lorentz forces. The Lorentz forces will create steel motion in the same direction of the rotating magnetic field.

There are many types of arrangement of coils and core geometry that create rotating fields. Most of them use the iron core with six coils around salient iron poles [10], [11]. The model of this work uses a toroidal coil winding.

III. MATHEMATICAL MODEL

The billet mold and the electromagnetic stirrer are represented in Fig. 1. The model contains about 120 000 elements. The air around the stirrer was omitted to show the details of the device. One can notice the iron core, the coils, the mold, and the steel billet. The mold curvature was not considered in this model because the magnetic field distribution has not changed much. The same does not happen with the fluid flow where the curvature has a significant effect on the flow profile and the inclusions distribution.

The ELEKTRA package uses a combination of vector and scalar magnetic potentials to model time-varying electromagnetic fields. In this model, the vector potential was used in conducting media, the reduced scalar potential in air media, and the total potential in the iron core media. The magnetic and the electric fields are related by the low-frequency limit of Maxwell's equations [9]

$$\text{Magnetic flux density: } \nabla \cdot \boldsymbol{B} = 0 \tag{1}$$

$$\text{Ampere's law: } J = \nabla \times \boldsymbol{H} \tag{2}$$

$$\text{Faraday's law: } \nabla \times \boldsymbol{E} = -\frac{\partial \boldsymbol{B}}{\partial \boldsymbol{t}} \tag{3}$$

and

$$\text{Ohm's law: } J = \sigma(E) \tag{4}$$

where σ is the electric conductivity, $\boldsymbol{B}$ is the magnetic flux density, $\boldsymbol{E}$ is the electric field strength, $\boldsymbol{H}$ is the magnetic field

TABLE I
SIMULATION DATA

Mold size	0.15 x 0.15 m
Mold length	0.8 m
Total length simulated	1.3 m
EMS position from the top of mold	0.6 m
EMS core length	0.2 m
EMS inner diameter	0.3 m
Number of phases	3
Current amplitude per phase	170A, 340A
Frequencies	3, 4, 5, 6 Hz
Copper mold conductivity (T=25°C)	4.7×10^7 (Ohm.m)$^{-1}$
Copper mold conductivity (T=150°C)	3.18×10^7 (Ohm.m)$^{-1}$
Molten steel conductivity	7.14×10^5 (Ohm.m)$^{-1}$
Iron core relative permeability	1000

strength, and J is the current density. The electromagnetic force density for each element is calculated by the relationship

$$F_{\text{time}} = J \times B \qquad (5)$$

where *time* is equal to $0°$ and $90°$ for real and imaginary parts, respectively. The time-average Lorentz force density is given by

$$F_{\text{ave}} = (F_0 + F_{90})/2. \qquad (6)$$

Boundary conditions are applied on the external surfaces of the external air. The position of these boundaries has been placed at a large distance from the billet and the iron core. The tangential magnetic condition $(\partial\phi/\partial n) = 0$ was applied at the edges of the air space surrounding the model, where n is the normal unit vector to the surface and ϕ is the reduced scalar potential. The three-phase coil excitation was applied. The design and operational are data together with the dimensions of the billet, and the electrical properties are given in Table I.

IV. EXPERIMENTAL DATA

The experimental data were obtained with a Gauss meter and an oscilloscope to measure the frequency range between 3 and 6 Hz. The data were obtained each 5 cm along the vertical distance in the mold and in the middle point of the section. Two values of current were considered: 170 and 340 A.

V. RESULTS AND DISCUSSION

Fig. 2 shows the magnetic flux density as a function of the vertical position in the billet mold for two values of current. The numerical results match well with the experimental measurements. The experimental data error is estimated to be in the order of 15%.

The z direction is shown in Fig. 1 and the starting point value in the graph corresponds to the mold top, as we can see in the figure to the left of the graph.

Fig. 3 shows the magnetic flux density peak as a function of frequency. The values are in agreement with the measured data.

Fig. 4 shows the time-average Lorentz force profile along the mold for the two values of current. We can note how the current intensity affects the forces distribution. When the current changes from 170 to 340 A, the force is multiplied by four.

In this figure, we can note the "second peak" that appears at the end of the copper mold. It occurs because the copper attenuates the magnetic field, creating a peak when the mold finishes.
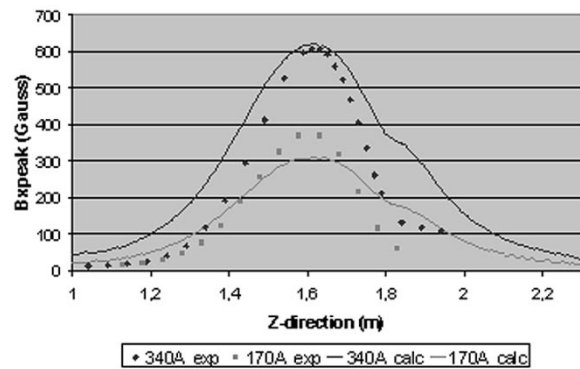

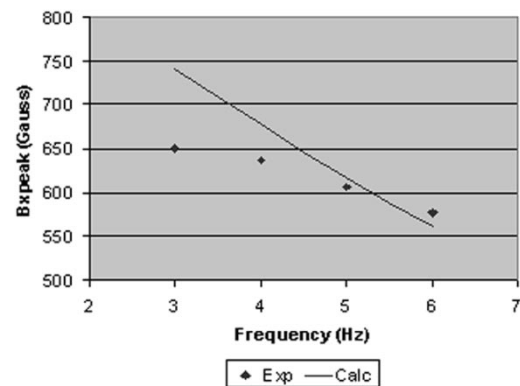Fig. 2. Magnetic flux density profile along the mold.

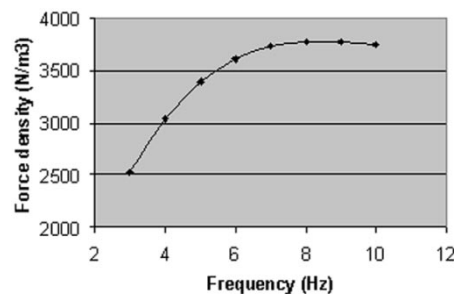
Fig. 3. Magnetic flux density peak versus frequency.

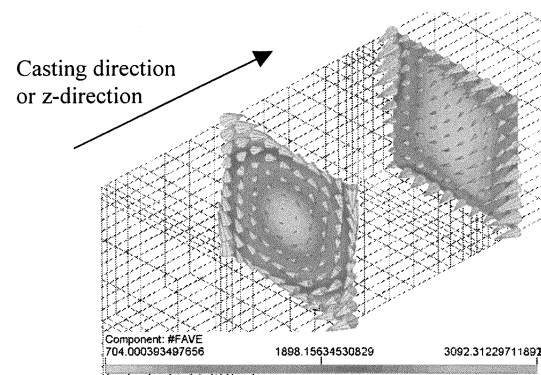Fig. 4. Time-average Lorentz force profile along the mold.

Fig. 5. Average Lorentz force vectors in N/m^3 along the mold.

The interesting nature of this peak can be analyzed through the components. This peak is mainly due to the z component of the force, as we can see in Fig. 5.

In Fig. 5, two planes along the mold are presented. The first is located in the center of the stirrer and the second at the end of the
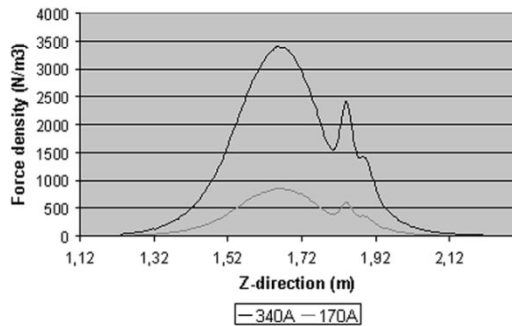
Fig. 6.   Relation between the maximum force density at the mold wall and frequency.
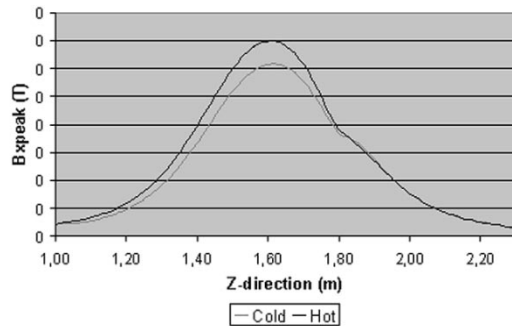

Fig. 7.   Magnetic flux density variation with temperature.

mold. The z component of the force appears to change the rotational movement. The main reason is that the real component of the z component of the force predominates over the imaginary part. This z component of the force will probably move the fluid upward. The consequences on the steel flow and the billet quality are still impossible to preview. The stirrer position in the mold also depends on the field intensity near the meniscus because it is common for slag entrapment to occur with excessive velocities in this region.

When the frequencies are analyzed, it is important to observe the torque produced by the stirrer. It is important because the mold is made of copper, which produces a maximum torque value.

Fig. 6 presents the relationship between the maximum force density close to the mold wall, i.e., the magnetic torque, and the frequency. We can note that the maximum torque occurs at 8-Hz frequency, although the magnetic flux density maximum value occurs at 3 Hz.

The temperature effect can be analyzed through the electrical conductivity of the mold. The electrical conductivity increases 1.4 times when the temperature decreases to about 125 °C. This variation affects the magnetic flux density as shown in Fig. 7. The difference between the peaks is almost 100 G.

VI. CONCLUSION

The numerical model was considered satisfactory to represent the electromagnetic stirrer effects. The numerical results are in agreement with the experimental data.

The numerical model shows the relationship between the current and the magnetic flux density and the force distribution. The copper mold attenuation is observed as a function of frequency and the torque. The temperature increase gives rise to a magnetic field increase.

After the model validation has been completed, we can apply the Lorentz force distribution in the molten steel.

REFERENCES

[1] A. A. Tzavaras and H. D. Brody, "Electromagnetic stirring and continuous casting— Achievements, problems, and goals," *J. Metals*, vol. 36, no. 3, pp. 31–37, 1984.
[2] J. P. Birat and J. Choné, "Electromagnetic stirring on billet, bloom, and slab continuous casting: State of the art in 1982," *Ironmaking Steelmaking*, vol. 10, no. 6, pp. 269–281, 1983.
[3] J.-L. Meyer, J. Szekely, and N. El-Kaddah, "Calculation of the electromagnetic force field for induction stirring in continuous casting," *Trans. ISIJ*, vol. 27, pp. 25–33, 1987.
[4] T. T. Natajaran and N. El-Kaddah, "Finite element analysis of electromagnetically driven flow in sub-mold stirring of billets and slabs," *ISIJ Int.*, vol. 38, no. 7, pp. 680–689, 1998.
[5] G. A. de Toledo, O. Campo, and E. Laínez, "Agitación electromagnética en la colada continua de acero," *Rev. Metal. Madrid*, vol. 31, no. 1, pp. 23–30, 1995.
[6] K. Fujisaki, T. Ueyama, T. Toh, M. Uehara, and S. Kobayashi, "Magneto hydrodynamic calculation for electromagnetic stirring of molten metal," *IEEE Trans. Magn.*, vol. 34, pp. 2120–2122, July 1998.
[7] K. Fujisaki, T. Ueyama, K. Takahashi, and S. Satoh, "Phase characteristics of electromagnetic stirring," *IEEE Trans. Magn.*, vol. 33, pp. 1642–1645, Mar. 1997.
[8] H. Hackl and P. J. Hanley, "The use and results of electromagnetic stirring for the continuous casting of steel," in *Proc. 50th Electric Furnace Conf.*, Nov. 1992, pp. 74–82.
[9] J. Szekely, *Fluid Flow Phenomena in Metals Processing*.   New York: Academic, 1979, pp. 175–203.
[10] F. C. Chang, J. R. Hull, and L. Beitelman, "Simulation of fluid flow induced by opposing AC magnetic fields in a continuous casting mold," in *Proc. 13th PTD Conf.*, 1995, pp. 79–88.
[11] F. Robiglio, A. Campos, J. Paiuk, M. Maldovan, J. Principe, A. Pignotti, and M. Goldschmit, "Diseño y modelado numerico del EMS en siderca," in *Proc. 12° Seminario de Acería del IAS y 2° Encuentro de la Sección Argentina de la Iron and Steel Soc.*, Nov. 1999, pp. 410–419.